X-ray radioluminescence effect of all-inorganic halide perovskite $CsPbBr_3$ quantum dots

Wang Chen, Yunpeng Liu, Zicheng Yuan, Zhiheng Xu, Zhengrong Zhang, Kai Liu, Zhangang Jin & Xiaobin Tang

Journal of Radioanalytical and Nuclear Chemistry
An International Journal Dealing with All Aspects and Applications of Nuclear Chemistry

ISSN 0236-5731
Volume 314
Number 3

J Radioanal Nucl Chem (2017)
314:2327-2337
DOI 10.1007/s10967-017-5562-x

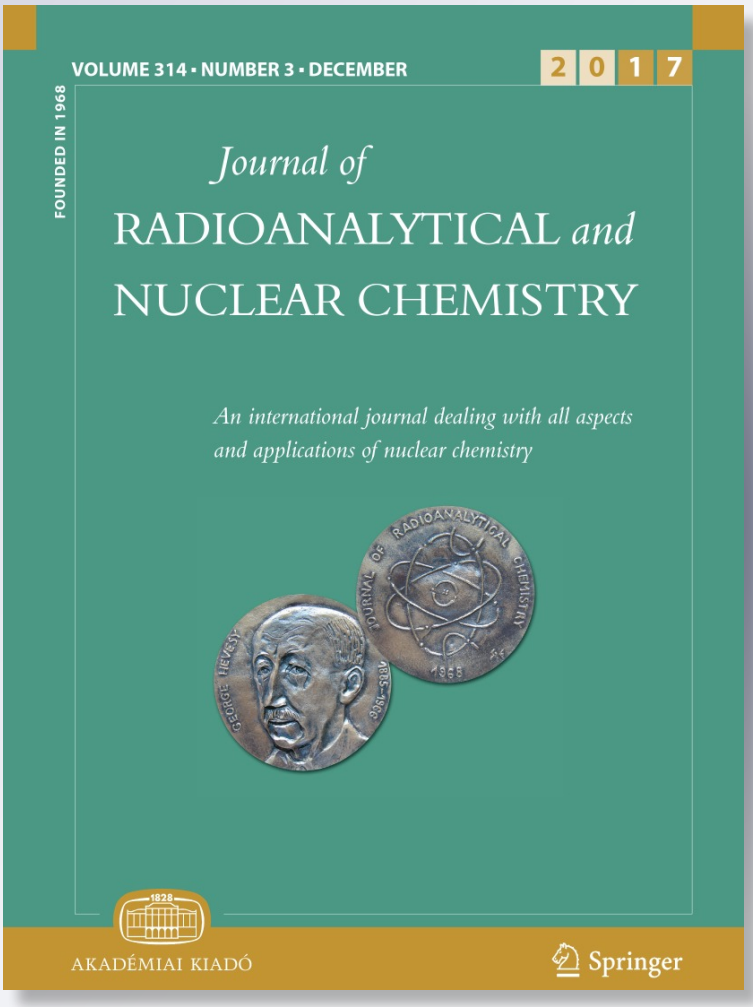

Springer

J Radioanal Nucl Chem (2017) 314:2327–2337
https://doi.org/10.1007/s10967-017-5562-x

X-ray radioluminescence effect of all-inorganic halide perovskite $CsPbBr_3$ quantum dots

Wang Chen[1] · Yunpeng Liu[1,2] · Zicheng Yuan[1] · Zhiheng Xu[1] · Zhengrong Zhang[1] · Kai Liu[1] · Zhangang Jin[1] · Xiaobin Tang[1,2]

Received: 9 September 2017 / Published online: 25 October 2017

Abstract $CsPbBr_3$ quantum dots (QDs) were synthesized with toluene and *n*-hexane as solvent by hot-injection method. Radioluminescence spectra of $CsPbBr_3$ QDs were characterized under different solvents, concentrations, and X-ray irradiation environments. The RL accounted for more than 18.1% of the total fluorescence of $CsPbBr_3$ QDs with toluene (10 mg/ml). The $CsPbBr_3$ QDs with *n*-hexane only showed RL under X-ray irradiation. Significant linear relationship was found between the RL relative intensity and tube current and solution concentration of $CsPbBr_3$ QDs. Thus, $CsPbBr_3$ QDs is promising scintillator material for X-ray scintillator detection and radioluminescent nuclear batteries.

Keywords $CsPbBr_3$ quantum dots · Radioluminescence effect · Linear response · X-ray scintillator

Introduction

Recent studies have focused on organic–inorganic hybrid perovskite materials, such as low-cost perovskite solar cells, with certified photo-conversion efficiency rapidly increased from 3.81 to 21% [1, 2]. This remarkable development has broken the monopoly of various traditional semiconductors. These organic–inorganic hybrid perovskite materials have been applied to photodetectors, field effect transistor, light-emitting diode [3, 4], laser, and memristor [5, 6] because of their unique optical and semiconducting characteristics. Owing to the rapid developments in perovskite materials, its application has rapidly been expanded to various fields. Thus, these materials have become a research hotspot for advance application to X-ray detectors.

In 2015, Yakunin reported a photoconductor with methyl ammonium triiodide (MAPbI3, MA = methylamine) as a highly sensitive photoconductor operated in the UV–visible, near-infrared, and soft X-ray spectral regions [7]. This photoconductor can be processed in a solution and used to directly convert the X-ray photon into current. In 2016, semiconductor hybrid lead halide perovskite ($MAPbI_3$, $MAPbBr_3$, and $FAPbI_3$; MA = methylamine and FA = formamidinium) obtained by 0.3–1 cm solution with single-crystal growth) has been demonstrated to be applicable to semiconductor radiation detectors [8].

In 2016, Birowosuto et al. successfully built a set of X-ray scintillator detectors with three types of single-crystal perovskites, namely, $MAPbI_3$, $MAPbBr_3$, and (EDBE) $PbCl_4$. The light output of these were recorded in 10–300 K, in which (EDBE) $PbCl_4$ reached maximum light output of 120,000 photons/MeV at 130 K, while $MAPbI_3$ and $MAPbBr_3$ reached maximum light output of 150,000 photons/MeV at 10 K [9]. Organic–inorganic hybrid perovskite material at appropriate operating temperature achieves 3–4 times the light output of widely used NaI (T1) scintillator (approximately 40,000 photons/MeV).

In 2013, Kanatzidis et al. reported the $CsPbBr_3$ single crystals which is a direct band gap semiconductor and the

Electronic supplementary material The online version of this article (doi:10.1007/s10967-017-5562-x) contains supplementary material, which is available to authorized users.

✉ Xiaobin Tang
tangxiaobin@nuaa.edu.cn

[1] Department of Nuclear Science and Engineering, Nanjing University of Aeronautics and Astronautics, 29 Yudao St, Nanjing 210016, China

[2] Jiangsu Key Laboratory of Material and Technology for Energy Conversion, 29 Yudao St, Nanjing 210016, China

high resistivity, high attenuation, and significant photoconductivity response. They considered $CsPbBr_3$ as a promising candidate material for X-ray detector which resolution is comparable to that of commercial [10]. Existing studies have shown that the stability of all-inorganic halide perovskite materials in solar cells and LED, among others, is better than that of organic–inorganic hybrid perovskite materials [11, 12]. Organic–inorganic hybrid perovskite materials have been successfully applied to X-ray detectors. These materials can also be applied in semiconductor and scintillator detectors. However, related studies on all-inorganic halide perovskite materials and their application in scintillator detectors have not been reported. In this paper, we report the $CsPbBr_3$ QDs in different solvent environments. The results demonstrate that X-ray can interact directly with $CsPbBr_3$ QDs to induce radioluminescence (RL) effect.

In 2016, Valais et al. reported an investigation of luminescence and radiation detection properties of the CdSe/ZnS quantum dots nanocrystals. The results demonstrated that the CdSe/ZnS quantum dots has great potential for detection of X-rays and medical imaging applications [13].

In this paper, we report the $CsPbBr_3$ QDs in different solvent environments. The results show that X-ray can interact directly with $CsPbBr_3$ QDs to induce radioluminescence (RL) effect. Based on the stability of the material to produce RL properties, all-inorganic halide perovskite $CsPbBr_3$ QDs were applied to the scintillator of an X-ray scintillator detector and the radioluminescent energy conversion material of radioluminescent nuclear batteries. Using these QDs in radioluminescent nuclear batteries is advantageous because of the feasibility of controlling the emission spectrum of the radioluminescent material by tuning the composition and size of all-inorganic halide QDs. This process results in a more suitable radioluminescent material for photovoltaic devices. Consequently, the energy conversion efficiency and output power of radioluminescent nuclear batteries can be remarkably improved [14–17].

Experimental

Synthesis of $CsPbBr_3$ QDs

All-inorganic halide perovskite QDs were synthesized using a hot-injection method with oleylamine (OAm) and oleic acid (OA) as surfactants [18]. The carboxyl and amine groups in OA and OAm were adsorbed or grafted onto the surface of the QDs during the reaction. Surface alkyl promotes the dispersion of $CsPbBr_3$ QDs in an organic solvent and disperses $CsPbBr_3$ QDs in common organic solvents, such as toluene and *n*-hexane.

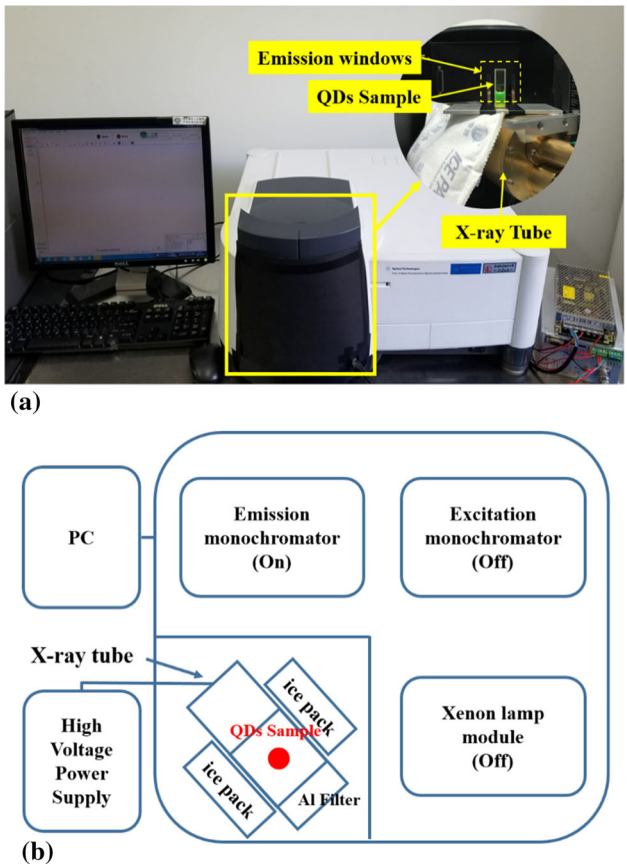

Fig. 1 **a** Physical diagram and **b** Schematic diagram of radioluminescence spectral measurement system

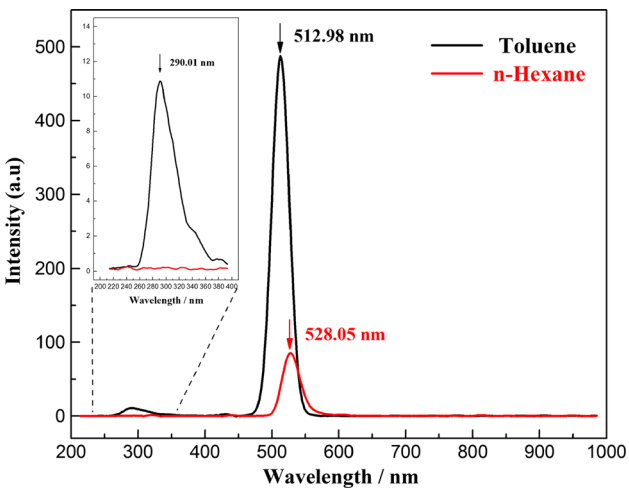

Fig. 2 RL spectra of $CsPbBr_3$ QDs (10 mg/mL) with toluene and *n*-hexane as solvent at 60 kV and 1000 μA

Methods

RL Spectra Measurement

The RL emission spectra of the $CsPbBr_3$ QD solutions were measured and characterized to determine the characteristic emission peaks of the solvent and solute. The X-ray source was an X-ray tube with a W target and operated at 10–60 kV and 100–1000 μA (Shanghai Key-Way Electron Company Ltd. KYW900A, China). A fluorescence spectrophotometer (Cary Eclipse Spectrometer, Agilent Technologies Inc., Malaysia) was used, and the emission spectrum is recorded for 200–1000 nm. The slit width of the emission monochromator was set to 20 nm, and the tube voltage of photomultiplier to 800 V. The physical and schematic diagrams of the RL spectral measurement system are shown in Fig. 1.

High-resolution transmission electron microscopy: One drop of $CsPbBr_3$ QD solution was dispersed onto a Cu grid. HRTEM images were taken on a Tecnai G2 F30 S-TWIN instrument.

Results and discussion

Characterization of $CsPbBr_3$ QDs

Two common organic solvents, namely, toluene and *n*-hexane, were used as solvents to synthesize the all-inorganic halide perovskite $CsPbBr_3$ QDs. The $CsPbBr_3$ QDs

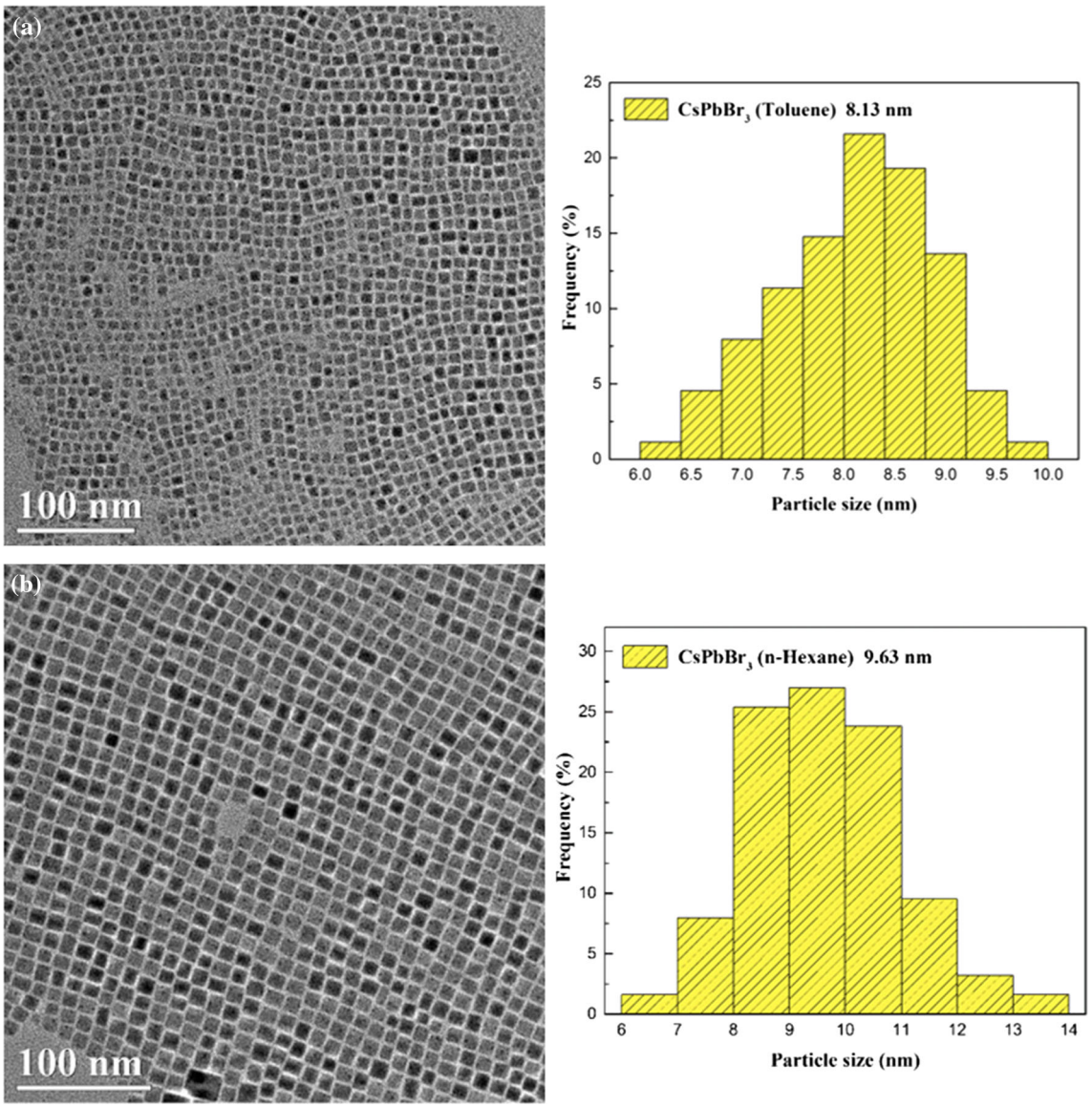

Fig. 3 High-resolution transmission electron microscopy (HRTEM) images and particle size distributions of $CsPbBr_3$ QD solutions with **a** toluene or **b** *n*-hexane as solvent

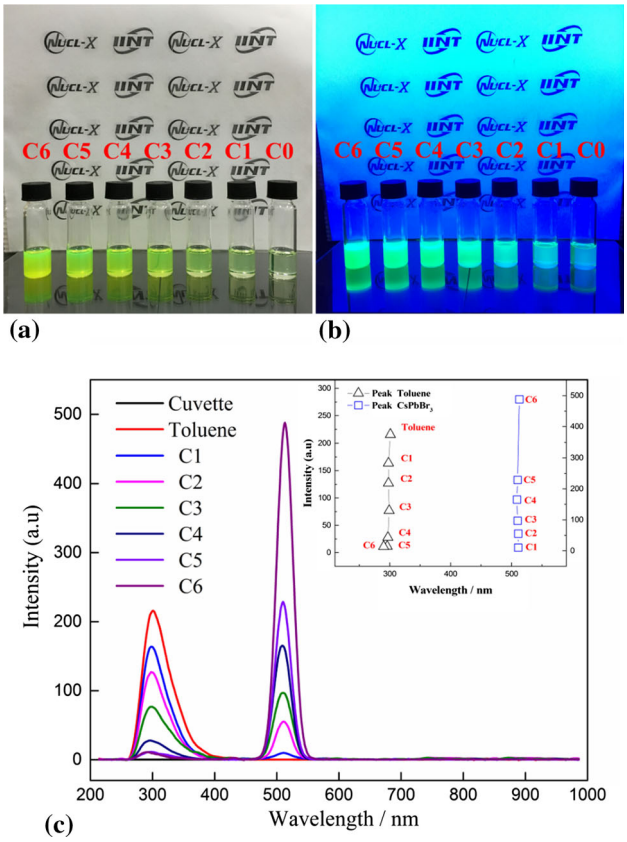

Fig. 4 **a** Different concentrations of $CsPbBr_3$ QDs solution in visible light: C1, 0.3125 mg/mL; C2, 0.625 mg/mL; C3, 1.25 mg/mL; C4, 2.5 mg/mL; C5, 5 mg/mL; and C6, 10 mg/mL. **b** Different concentrations of $CsPbBr_3$ QDs solution under 365 nm UV lamps. **c** The RL spectra of an empty cuvette, toluene, and $CsPbBr_3$ QDs of different concentrations at 60 kV and 1000 μA

were prepared using hot-injection method under two different solvent environments. Only the solvent differed in the centrifugation and dispersion step.

The RL spectra of the $CsPbBr_3$ QD solutions with identical concentrations (10 mg/mL) but different solvents were compared at 60 kV and 1000 μA (maximum X-ray energy and maximum X-ray flux in the experiment; Fig. 2).

The peak position of the RL spectrum of $CsPbBr_3$ QDs with *n*-hexane is 528.05 nm, while that of $CsPbBr_3$ QDs with toluene is 512.98 nm. The emission spectrum of toluene has a wide emission spectrum near 300 nm. This phenomenon is observed in the RL spectrum of $CsPbBr_3$ QDs with toluene at different concentrations and X-ray irradiation environments. However, this phenomenon is not observed in the RL spectrum of $CsPbBr_3$ QDs with *n*-hexane. The emission peak positions of the RL spectra of the two distinct $CsPbBr_3$ QD solutions differ because of the varied particle sizes of the quantum dots [18, 19]. HRTEM images and results from the particle size analysis of the two $CsPbBr_3$ QDs solutions are presented in Fig. 3.

HRTEM images show distinct particle sizes of the two synthesized QDs. The difference in the reaction conditions during synthesis primarily causes the difference in the emission peak position of the RL spectra of the two different $CsPbBr_3$ QD solutions.

$CsPbBr_3$ QDs with toluence solvent

RL spectrum

The tube voltage of the X-ray tube was 10–60 kV, at increment of 10 kV, and tube current was 100–1000 μA, at increment of 100 μA. The RL emission spectra of $CsPbBr_3$ QDs solution with different concentrations of C1–C6 were tested. The spectra at 60 kV and 1000 μA is illustrated in Fig. 4. The experimental solution (1.5 mL) was compared with toluene solution (AR) with identical volume. Sample C0 (∼ 0.156 mg/mL) was discarded, because the characteristic peak of the RL spectrum of the $CsPbBr_3$ QDs was not obvious as shown at the right ends of Fig. 4a and b.

The experimental results show that the toluene solution at different tube currents and tube voltages has an emission peak near 300 nm. Another emission peak appears near 300 nm in all $CsPbBr_3$ QDs solution with toluene. The molecular structure of toluene contains benzene rings. The molecular structure of the organic matter that produces fluorescence generally contains conjugated double or π bonds. The larger of the conjugated system is, the more easily the delocalized π is excited, and the more easily fluorescence occurs. Most fluorescent materials have aromatic or heterocyclic rings. For example, benzene and naphthalene fluorescence are located in the UV region. Anthracene is located in the blue zone [20]. Thus, based on the theoretical basis and experimental results, the peak of the RL emission spectrum near 300 nm is attributed to the RL of toluene.

The results show two significant emission peaks in the RL emission spectra of $CsPbBr_3$ QD solutions with different concentrations. One of the peaks of the emission peak is identical to the RL peak of toluene. The peaks position and peak values in the RL spectrum of the C1–C6 samples are illustrated in Fig. 4. The peak profile matching of the RL spectrum emission peaks at 255–400 nm was obtained by the normalized spectrum in Fig. S1 (Supporting Information), and samples with different concentrations of C1–C6 were analyzed. The peak value of the characteristic peak of the QDs increases with the concentration of $CsPbBr_3$ QDs solution. The peak value is changed from below the toluene characteristic peak value to higher than this value. For $CsPbBr_3$ QDs solutions with toluene, there may be two physical processes that result in the characteristic fluorescence of

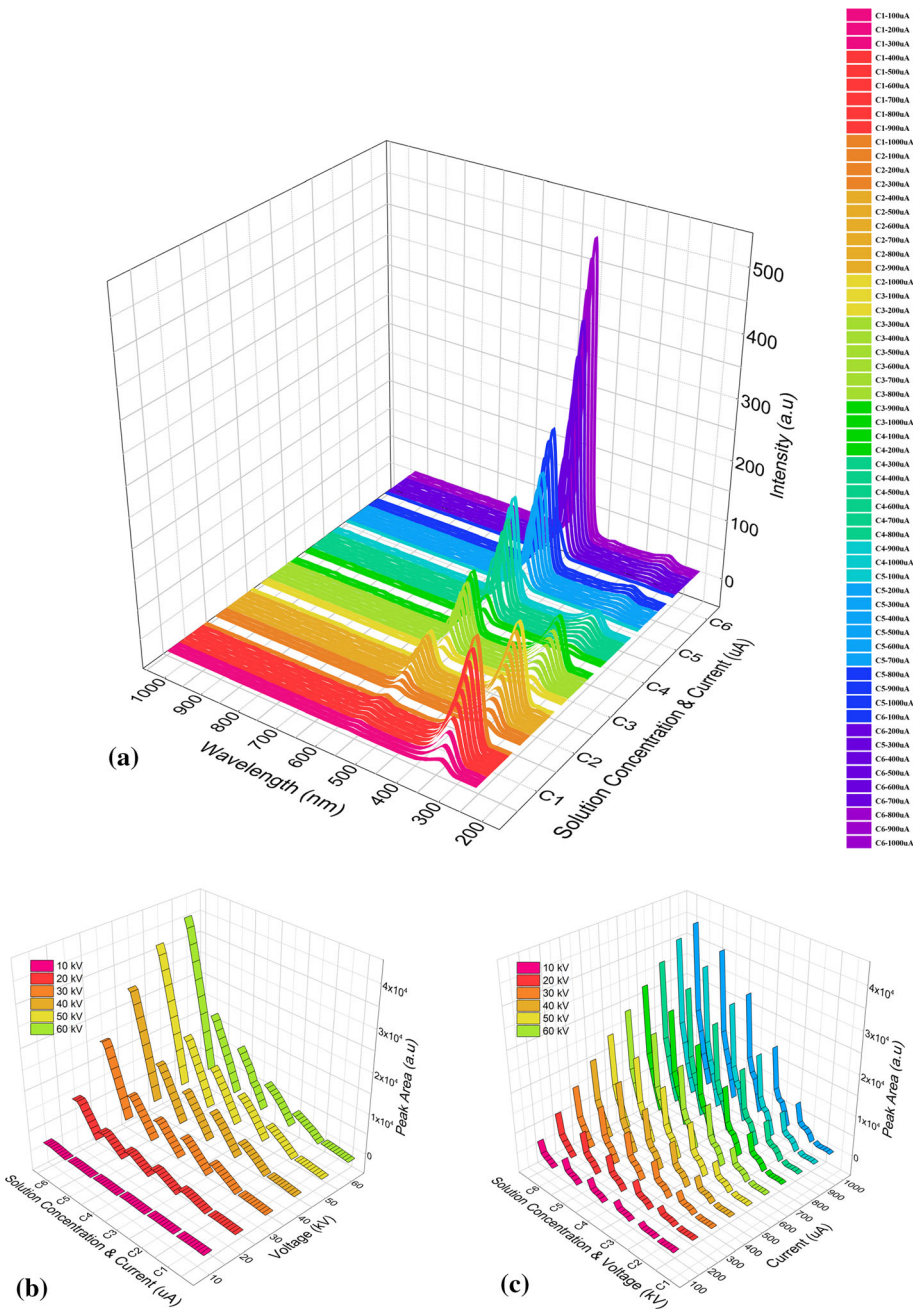

Fig. 5 **a** Emission spectra of C1–C6 with toluene at the tube voltage of 60 kV and tube current of 100–1000 μA. $CsPbBr_3$ emission peak areas with variations in **b** tube current and **c** tube voltage

$CsPbBr_3$ QDs under X-ray irradiation. X-ray interacts directly with toluene to produce UV light near 300 nm. In addition to that, the fluorescence of $CsPbBr_3$ QDs contains the photoluminescence (PL) of $CsPbBr_3$ QDs by UV light and the radioluminescence (RL) of $CsPbBr_3$ QDs by X-ray.

Whether X-ray can directly act on $CsPbBr_3$ QDs in the $CsPbBr_3$ QD solution with toluene was quantitatively analyzed. Moreover, the ratios of the PL and RL of the $CsPbBr_3$ QDs solutions with toluene were determined.

Variation in the RL spectrum of $CsPbBr_3$ QDs with X-ray parameters

The RL spectra of $CsPbBr_3$ QDs with different concentrations of C1–C6 were investigated at different X-ray irradiation environments (tube voltage of 10–60 kV and tube current of 100–1000 μA). The RL spectra of 360 experimental groups were analyzed. The responses of RL relative intensity of $CsPbBr_3$ QDs to concentration, tube voltage, and tube current were determined. The RL spectra of $CsPbBr_3$ QDs with fixed tube voltage of 60 kV, tube

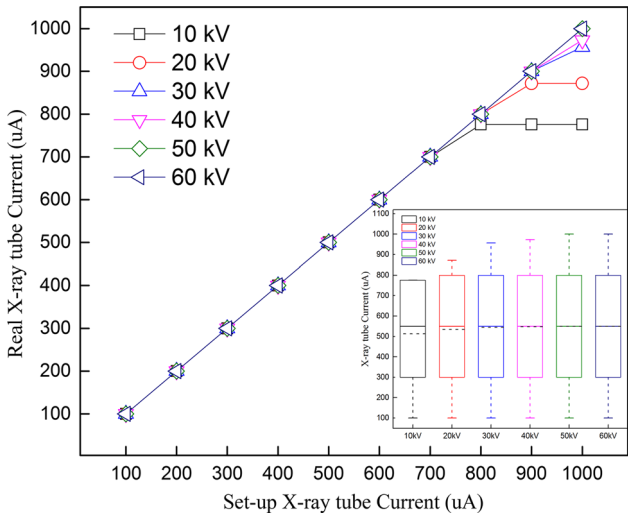

Fig. 6 Real tube current curve of the X-ray tube under different tube voltages (10–60 kV)

currents of 100–1000 μA, and different concentrations of C1–C6 are illustrated in Fig. 6. The *x*-axis of the RL spectrum of the $CsPbBr_3$ QDs is transformed according to Eq. (1) [21]. Then, the full spectral integral areas of the characteristic emission spectra of toluene and $CsPbBr_3$ QDs were calculated accordingly. Under identical experimental conditions, the emission peak area can be equivalent to the RL relative intensity. The relationships between RL relative intensity and X-ray tube current, tube voltage, and concentration were analyzed.

$$E = hv,\ \lambda \cdot v = c,\ \Rightarrow E = hc/\lambda \Rightarrow E(\text{eV}) = 1239.6/\lambda(\text{nm}) \quad (1)$$

The RL spectra of C1–C6 in different X-ray irradiation environments with toluene as solvent show two significant characteristic emission peaks (Fig. 5a). Two characteristic emission peaks are at ~ 300 nm for toluene and at ~ 512.98 nm for the $CsPbBr_3$ QDs. The RL relative

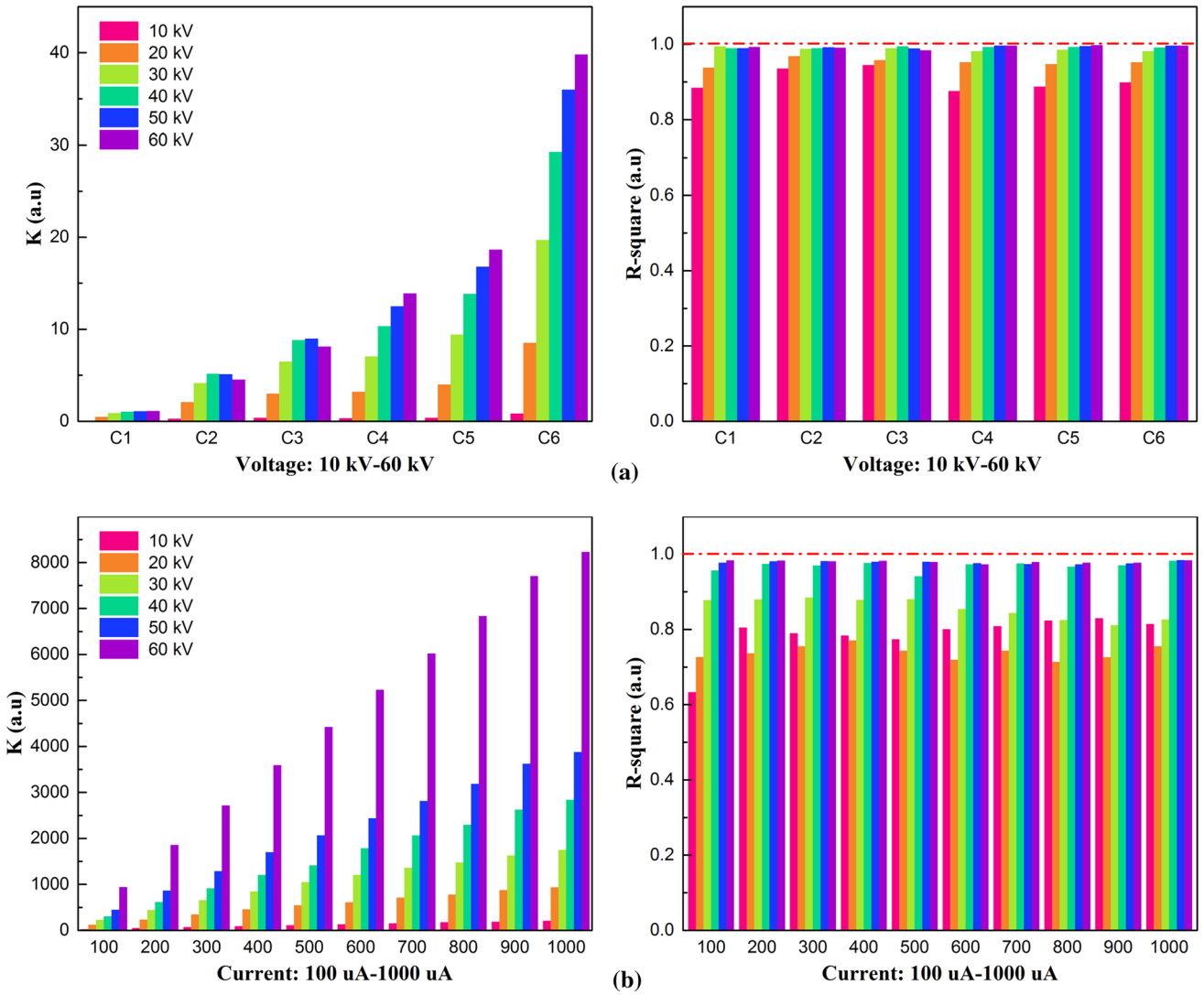

Fig. 7 The slopes, *K* values, and R^2 values of the linear fitting of $CsPbBr_3$ QDs emission peak area to **a** tube current and **b** concentration

intensity (RL emission peak area) of the $CsPbBr_3$ QDs is proportional to the response of the tube voltage and tube current and linearly related to the tube current (Fig. 5b, c). This linear relationship was further investigated under different tube voltages and concentrations. Given the output power limitation of the X-ray tube, the real tube current of the X-ray tube is inconsistent with the set tube current at the lower tube voltage (Fig. 6; the box-plot of the real tube current under the various tube voltages).

The X-ray tube used in the experiment cannot achieve a current of 1000 μA at tube voltages of 10, 20, 30, and 40 kV, because of the output power limitation (Fig. 6). The deviation from the real tube current explains the gentle variation in the emission peak areas of the $CsPbBr_3$ QDs near the maximum tube current at different concentrations of C1–C6 at low tube voltage (Fig. 5b).

The R-square value is generally less than 0.9 at tube voltage of 10 kV because of the deviation from the real tube current. However, these values are generally greater than 0.9 at tube voltages of 20–60 kV. The emission peak area of $CsPbBr_3$ QDs is well fitted with the tube current, and emission peak area of $CsPbBr_3$ QDs is linearly related

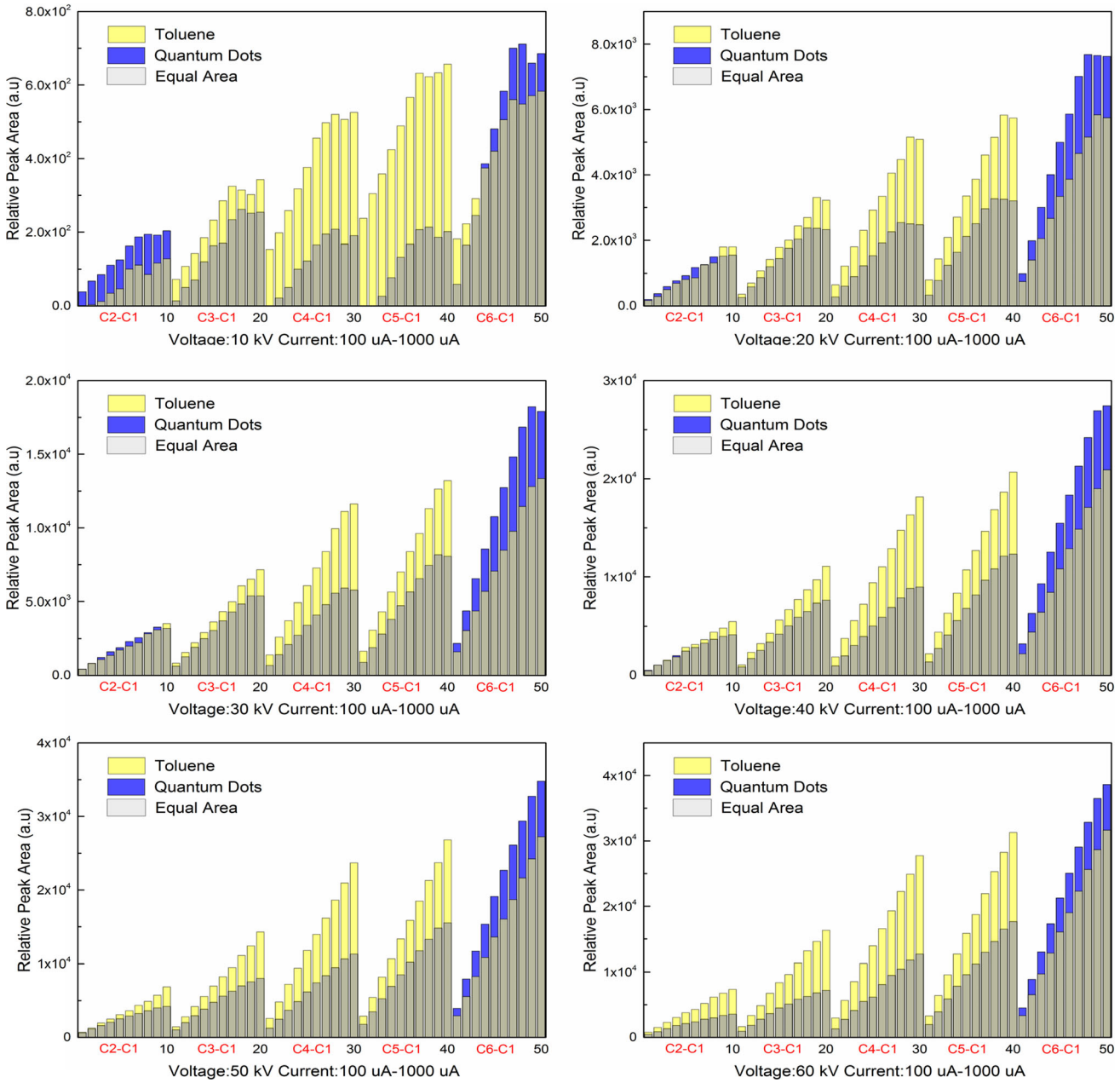

Fig. 8 Relative peak area of $CsPbBr_3$ QDs and toluene emission peak at the tube voltage of 10–60 kV (Bar graph: yellow bar represents the relative peak area of the toluene, blue bar represents the relative peak area of the $CsPbBr_3$ QDs, and the gray bar represents the peak equal area)

to concentration. The specific values are shown in Tables S2 and S3 (Supporting Information) (Fig. 7).

The relative variations in the peak areas of the characteristic emission peaks of toluene and $CsPbBr_3$ QDs under different concentrations and identical X-ray irradiation environments were compared. The ratios of RL and PL in the RL emission spectra of $CsPbBr_3$ QDs under different X-ray irradiation environments were determined for quantitative analysis. The concentration of C1 (0.3125 mg/mL) was used as a reference. The characteristic peak area of toluene and $CsPbBr_3$ QDs of reference sample C1 were subtracted from those of C2–C6 with different concentrations to obtain the relative peak areas of toluene and $CsPbBr_3$ QDs with different concentrations of C2–C6. These relative peak areas were analyzed under different tube voltages of 10–60 kV (Fig. 8).

At 10 kV, the average energy of X-ray emitted by the X-ray tube is lower, and the current is less than 1000 μA. Although the linearity of the experimental data before 700 μA is significant, the $CsPbBr_3$ QDs characteristic emission peak is not clearly characterized because of the low average X-ray energy and unattained tube current value. The experimental results under 10 kV are not representative and cannot be used for comparative analysis. By contrast, at tube voltages of 20–60 kV, C1–C6 samples, relative peak areas of the characteristic emission peaks of toluene and $CsPbBr_3$ QDs show a significant linear relationship with tube current. For the C6 sample (10 mg/mL), the relative peaks of $CsPbBr_3$ QDs are generally higher than the relative peak area of toluene under different tube voltages (20–60 kV) and tube current (100–1000 μA).

The fluorescence emitted by $CsPbBr_3$ QD solution under different X-ray irradiation environments, including toluene RL, the $CsPbBr_3$ QDs PL by the UV light of toluene, and other exciting forms. Additional forms of excitation are considered to be contributed by the X-rays directly acting on the $CsPbBr_3$ QDs which induced RL effects (the additional fluorescence is presumed to be the contribution of

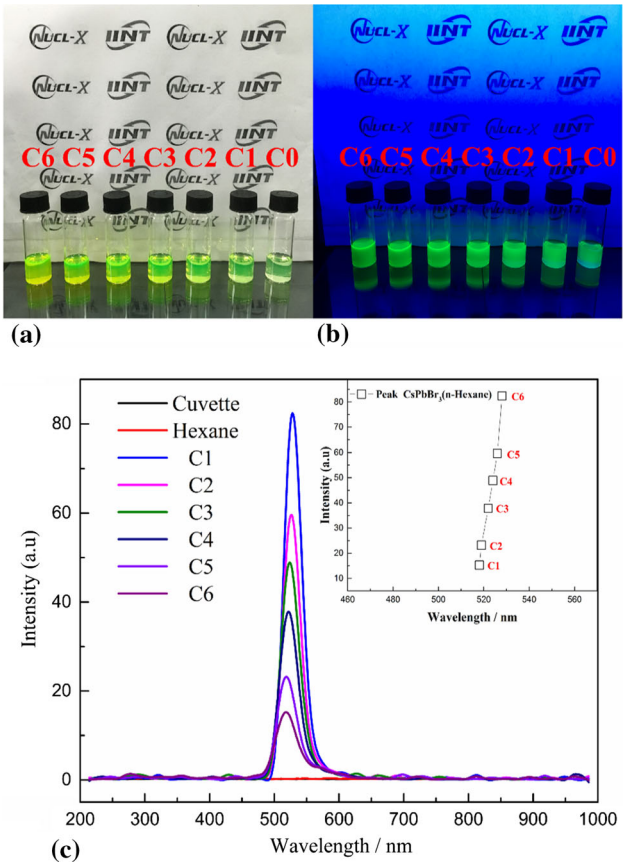

Fig. 9 **a** Different concentrations of $CsPbBr_3$ QDs solution in visible light: C1, 0.3125 mg/mL; C2, 0.625 mg/mL; C3, 1.25 mg/mL; C4, 2.5 mg/mL; C5, 5 mg/mL; and C6, 10 mg/mL. **b** Different concentrations of $CsPbBr_3$ QDs solution under 365 nm UV lamps. **c** The RL spectra of an empty cuvette, toluene, and $CsPbBr_3$ QDs of different concentrations at 60 kV and 1000 μA

Table 1 Ratios of radioluminescence (RL) to total fluorescence in sample C6 (10 mg/L)

Current (μA)	Voltage (kV)				
	20 RL[a]/(PL[b] + RL) (%)	30 RL/(PL + RL) (%)	40 RL/(PL + RL) (%)	50 RL/(PL + RL) (%)	60 RL/(PL + RL) (%)
100	24.28	26.48	31.35	25.53	26.21
200	29.03	30.59	30.16	29.94	26.46
300	31.82	33.17	30.78	29.26	25.48
400	33.48	33.62	32.79	29.58	25.86
500	33.17	34.34	30.09	28.88	24.38
600	34.02	33.40	29.73	29.23	24.09
700	33.68	34.13	30.23	28.41	23.27
800	32.87	32.03	29.44	26.39	21.98
900	23.71	29.76	29.53	25.98	21.48
1000	24.62	25.51	23.79	21.76	18.10

RL[a]: ratio of the RL produced by the $CsPbBr_3$ QDs to the total fluorescence. PL[b]: ratio of the PL produced by the $CsPbBr_3$ QDs to the total fluorescence

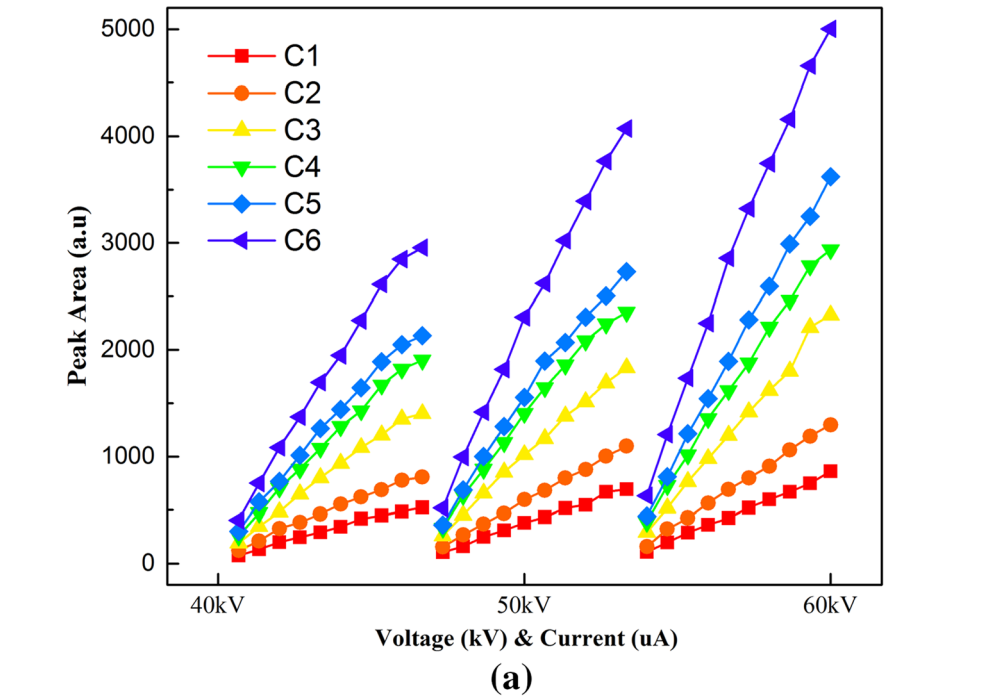

(a)

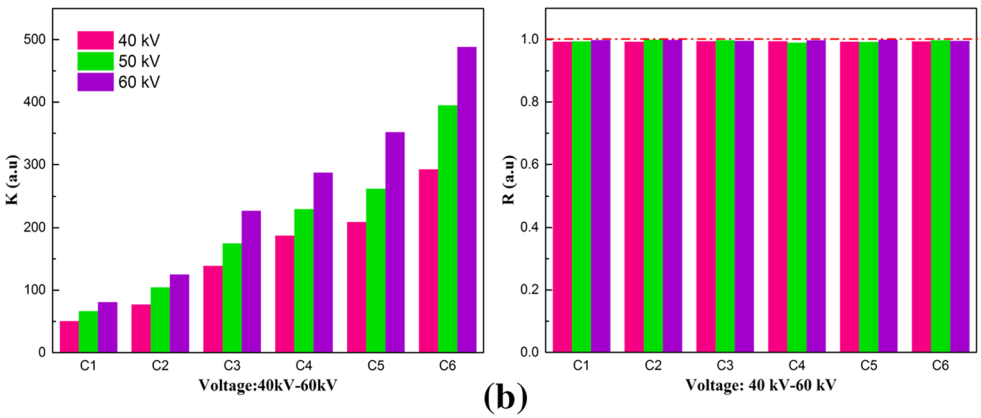

(b)

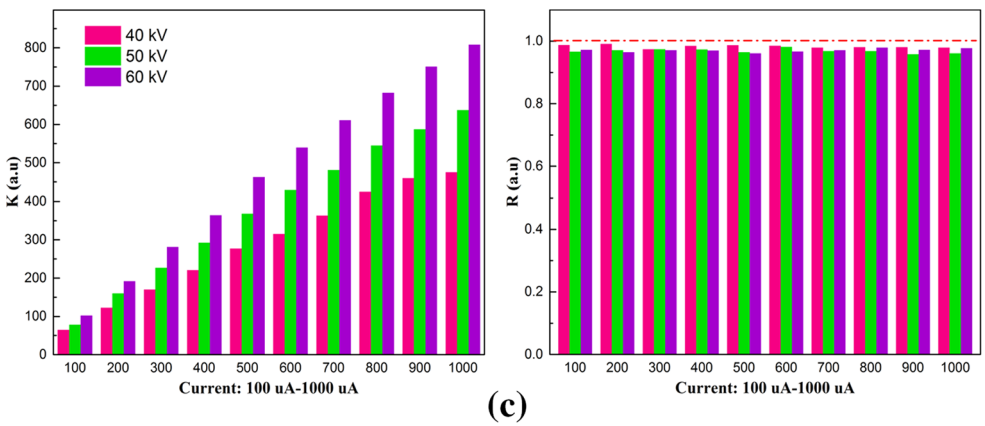

(c)

Fig. 10 **a** $CsPbBr_3$ emission peak area with *n*-hexane as solvent. The slopes, *K* values, and R^2 values of the linear fitting of $CsPbBr_3$ QDs emission peak area to **b** tube current and **c** concentration

RL effects). Additional forms of excitation are considered to be contributed by the X-rays directly acting on the $CsPbBr_3$ QDs which induced RL effects (the additional fluorescence is presumed to be the contribution of RL effects). The photons emitted by toluene can be completely transformed by the $CsPbBr_3$ QDs (assuming that the quantum efficiency of the $CsPbBr_3$ QDs is 100%, and the quantum efficiency of the actual $CsPbBr_3$ QDs is approximately 88%). The effect of X-rays directly acting on the $CsPbBr_3$ QDs in inducing RL effects can be fully proved. For sample C6 (10 mg/mL), the ratios of the fluorescence produced by the RL to the total fluorescence (PL + RL) under 20–60 kV and 100–1000 μA are shown in Table 1.

The results show that the ratio of $CsPbBr_3$ QDs RL is more than 18.1% under 20–60 kV and 100–1000 μA. *N*-hexane was selected as solvent for more in-depth studies to directly demonstrate that X-ray can directly act on the $CsPbBr_3$ QDs to induce RL effect.

$CsPbBr_3$ QDs with *n*-hexane solvent

Based on the study with toluene solvent, *n*-hexane was selected as solvent under 40–60 kV and 100–1000 μA for further study. The RL emission spectra of $CsPbBr_3$ QDs solutions with different concentrations of C1–C6 at 60 kV and 1000 μA are illustrated in Fig. 9. The experimental solution (1.5 mL) was compared with *n*-hexane solution (AR) with identical volume. Sample C0 ($\sim$ 0.156 mg/mL) was discarded, because the characteristic peak of the RL spectrum of the $CsPbBr_3$ QDs was not obvious as shown at the right ends of Fig. 9a and b.

The RL spectra of C1–C6 samples with *n*-hexane as solvent show only one significant characteristic emission peak under different X-ray irradiation environments (Fig. 9c). The characteristic emission peak of $CsPbBr_3$ QDs is found near 528.05 nm. Figure 10b and c show that the fluorescence intensity of the $CsPbBr_3$ QDs with different concentrations is proportional to the X-ray tube voltage and tube current and linearly related to the tube current. These results are consistent with the experimental results with toluene as solvent. The linear relationship between the RL relative intensity and tube current with different concentrations of $CsPbBr_3$ QDs is illustrated in Fig. 10b, c.

The linear fitting results show that the R-square values of the $CsPbBr_3$ QDs with *n*-hexane are more than 0.99, and the $CsPbBr_3$ QDs emission peak area has a significant linear relationship with the tube current at 40, 50, and 60 kV. Significant linear relationship is also found between the peak area and concentration of $CsPbBr_3$ QD solutions. The specific values are shown in Tables S4 and S5 (Supporting Information). In the previous discussion, the additional fluorescence with toluene solvent is assumed to contribute to the RL effect of the $CsPbBr_3$ QDs. The results with *n*-hexane as solvent prove that X-ray can directly act on the $CsPbBr_3$ QDs to induce RL effect.

Conclusions

$CsPbBr_3$ QDs with toluene or *n*-hexane as solvent were synthesized by hot-injection method, and the HRTEM images show that the resulting particle sizes are 8.13 nm and 9.63 nm, respectively. The specific physical processes of $CsPbBr_3$ QDs solution with different concentrations under distinct X-ray irradiation environments (various tube currents and voltages) were investigated. The results confirm that the emission spectrum near 300 nm in the RL spectrum of the $CsPbBr_3$ QDs solution with solvent is derived from the RL of the toluene solvent. The emission spectrum near 512 nm is derived from the PL and RL of the $CsPbBr_3$ QDs.

Moreover, the RL relative intensity of $CsPbBr_3$ QDs of the C6 sample (10 mg/mL) with toluene is much larger than that of toluene solvent under different X-ray irradiation environments. X-ray (tube voltage of 20–60 kV and a tube current of 100–1000 μA) can directly act on the $CsPbBr_3$ QDs to induce RL effect, which accounts for more than 18.1% of the total fluorescence produced by $CsPbBr_3$ QDs. With *n*-hexane as a solvent, the emission spectrum appears only in the RL spectrum of the $CsPbBr_3$ QD solutions. Thus, the fluorescence of the dots is completely generated by RL. $CsPbBr_3$ QDs with toluene or *n*-hexane show a significant linear relationship between RL relative intensity and tube current and solution concentration.

The $CsPbBr_3$ QD solution with toluene or *n*-hexane shows a significant linear response to the 20–60 kV beam current. Thus, the $CsPbBr_3$ QDs is a promising scintillator material for X-ray scintillation detectors and radioluminescent nuclear batteries. A scintillation material that matches the peak wavelength of the photomultiplier tube should be synthesized for scintillator detectors. The FWHM of the spectrum is approximately 30 nm, which is much smaller than that of widely used scintillator materials. These characteristics are beneficial in improving the overall performance of scintillator detectors. Consequently, more suitable radioluminescent material for PV device can be obtained. The proposed process can effectively improve the energy conversion efficiency and output power of radioluminescent nuclear batteries. The X-ray energy response for $CsPbBr_3$ QDs was not studied in detail. The relationship between $CsPbBr_3$ QDs RL effect and X-ray energy response and the RL effect of $CsPbBr_3$ QDs with charged particles α and β will be further examined.

Acknowledgements The authors would like to acknowledge the support of the National Natural Science Foundation of China (Grant No. 11675076 and 11505096), the National Defense Basic Scientific Research Project (Grant No. JCKY2016605C006), the Natural Science Foundation of Jiangsu Province (Grant No. BK20141406 and BK20150735), the Shanghai Aerospace Science and Technology Innovation Project (Grant No. SAST2016112), the Foundation of Graduate Innovation Center in NUAA (Grant No. kfjj20170611), and the Priority Academic Programme Development of Jiangsu Higher Education Institutions. *Wang Chen, *Yunpeng Liu. These authors contributed to the work equally and should be regarded as co-first authors.

References

1. Kida N, Hikita M, Kashima I et al (2009) Control of charge transfer phase transition and ferromagnetism by photoisomerization of spiropyran for an organic-inorganic hybrid system, (SP)[$Fe^{II}Fe^{III}$(dto)3] (SP = spiropyran, dto = $C_2O_2S_2$). J Am Chem Soc 131:212–220. doi:10.1021/ja806879a
2. Jeon NJ, Noh JH, Yang WS et al (2015) Compositional engineering of perovskite materials for high-performance solar cells. Nature 517:476–480. doi:10.1038/nature14133
3. Byun J, Cho H, Wolf C et al (2016) Efficient visible quasi-2D perovskite light-emitting diodes. Adv Mater. doi:10.1002/adma.201601369
4. Cho H, Jeong S-H, Park M-H et al (2015) Overcoming the electroluminescence efficiency limitations of perovskite light-emitting diodes. Science 350:1222–1225. doi:10.1126/science.aad1818
5. Kim Y-H, Cho H, Lee T-W (2016) Metal halide perovskite light emitters. Proc Natl Acad Sci 113:11694–11702. doi:10.1073/pnas.1607471113
6. Dou L, Yang Y, You J et al (2014) Solution-processed hybrid perovskite photodetectors with high detectivity. Nat Commun 5:5404. doi:10.1038/ncomms6404
7. Yakunin S, Sytnyk M, Kriegner D et al (2015) Detection of X-ray photons by solution-processed lead halide perovskites. Nat Photonics 9:444–449. doi:10.1038/nphoton.2015.82
8. Yakunin S, Dirin DN, Shynkarenko Y et al (2016) Detection of gamma photons using solution-grown single crystals of hybrid lead halide perovskites. Nat Photonics 10:585–589. doi:10.1038/nphoton.2016.139
9. Birowosuto MD, Cortecchia D, Drozdowski W et al (2016) X-ray scintillation in lead halide perovskite crystals. Sci Rep 6:37254. doi:10.1038/srep37254
10. Stoumpos CC, Malliakas CD, Peters JA et al (2013) Crystal growth of the perovskite semiconductor CsPbBr 3: a new material for high-energy radiation detection. Cryst Growth Des 13:2722–2727. doi:10.1021/cg400645t
11. Li X, Wu Y, Zhang S et al (2016) $CsPbX_3$ Quantum Dots for lighting and displays: roomerature synthesis, photoluminescence superiorities, underlying origins and white light-emitting diodes. Adv Funct Mater 26:2435–2445. doi:10.1002/adfm.201600109
12. Swarnkar A, Marshall AR, Sanehira EM et al (2016) Quantum dot-induced phase stabilization of -CsPbI3 perovskite for high-efficiency photovoltaics. Science 354:92–95
13. Nikolopoulos D, Valais I, Michail C et al (2016) Radioluminescence properties of the CdSe/ZnS Quantum Dot nanocrystals with analysis of long-memory trends. Radiat Meas 92:19–31. doi:10.1016/j.radmeas.2016.06.004
14. Hong L, Bin Tang X, Xu ZH et al (2014) Parameter optimization and experiment verification for a beta radioluminescence nuclear battery. J Radioanal Nucl Chem 302:701–707. doi:10.1007/s10967-014-3271-2
15. Xu ZH, Bin Tang X, Hong L et al (2015) Structural effects of ZnS: Cu phosphor layers on beta radioluminescence nuclear battery. J Radioanal Nucl Chem 303:2313–2320. doi:10.1007/s10967-014-3655-3
16. Prelas MA, Popovici G, Khasawinah S, Sung J (1995) In: Prelas MA, Gielisse P, Popovici G, Spitsyn BV, Stacy T (eds) Wide band-gap photovoltaics. Kluwer Academic Publishers, Dordrecht
17. Sychov M, Kavetsky A, Yakubova G et al (2008) Alpha indirect conversion radioisotope power source. Appl Radiat Isot 66:173–177. doi:10.1016/j.apradiso.2007.09.004
18. Song J, Li J, Li X et al (2015) Quantum dot light-emitting diodes based on inorganic perovskite cesium lead halides ($CsPbX_3$). Adv Mater 27:7162–7167. doi:10.1002/adma.201502567
19. Protesescu L, Yakunin S, Bodnarchuk MI et al (2015) Nanocrystals of cesium lead halide perovskites ($CsPbX_3$, X = Cl, Br, and I): novel optoelectronic materials showing bright emission with wide color gamut. Nano Lett. doi:10.1021/nl5048779
20. Schram E, Lombaert R (1963) Organic scintillation detectors. Elsevier Publishers, Amsterdam
21. Ang BG, Schotte F (2015) Photochemistry governing bacteriorhodopsin and bacterial reaction center. doi:10.13140/RG.2.1.1373.1363